AD-A090 116 NAVAL RESEARCH LAB WASHINGTON DC F/G 18/1
LASER FUSION STUDIES AT NRL.(U)
OCT 80 J MCMAHON, J ORENS, S BODNER, D BOOK
UNCLASSIFIED NRL-MR-4350 NL

1 OF 1
AD-A090116

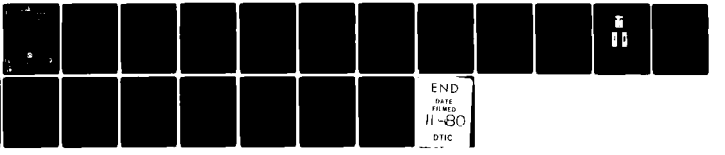

END
DATE FILMED
11-80
DTIC

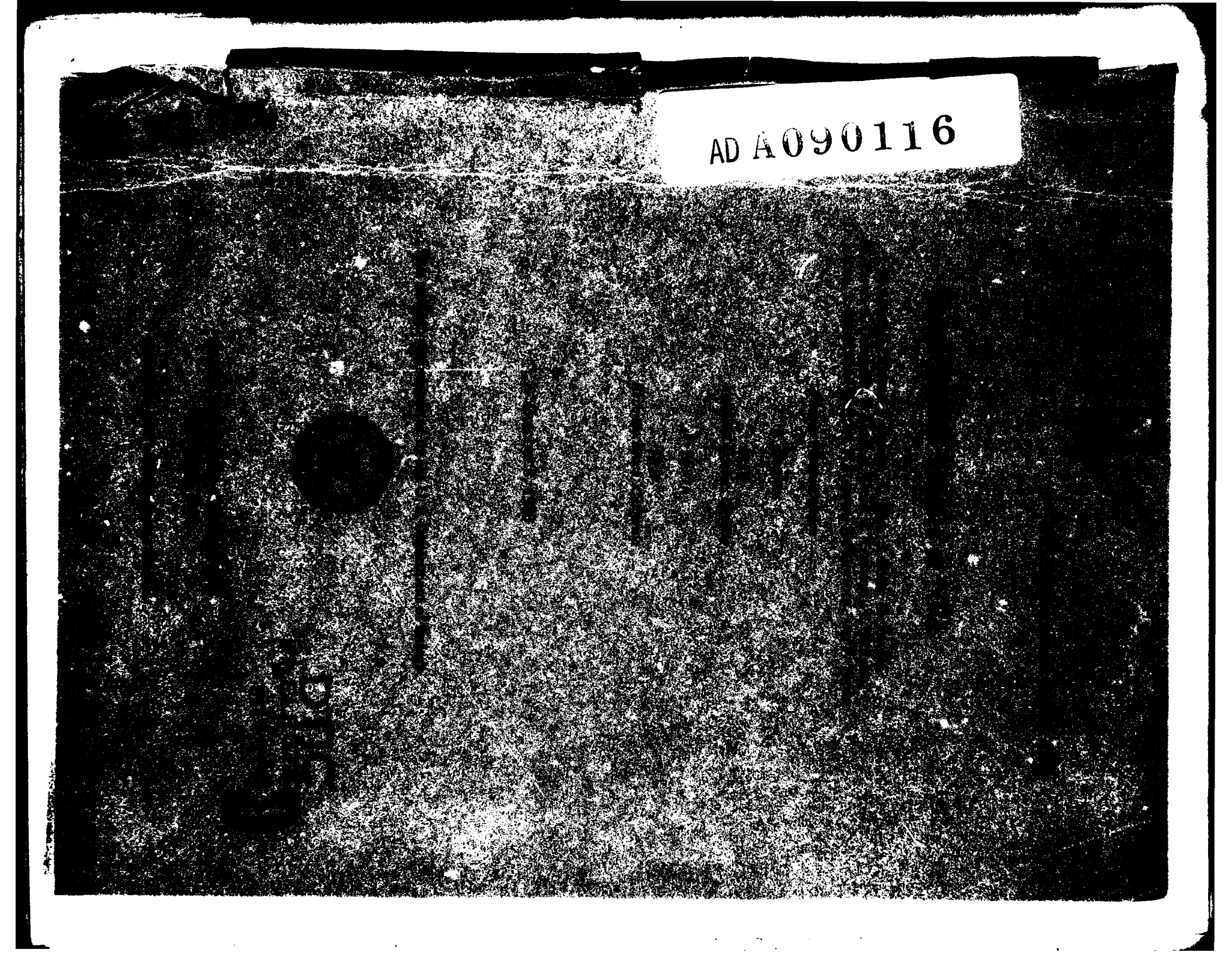

SECURITY CLASSIFICATION OF THIS PAGE (When Data Entered)

REPORT DOCUMENTATION PAGE		READ INSTRUCTIONS BEFORE COMPLETING FORM
1. REPORT NUMBER (14) NRL-MR- NRL Memorandum Report 4359	2. GOVT ACCESSION NO. AD-A090 116	3. RECIPIENT'S CATALOG NUMBER
4. TITLE (and Subtitle) (6) LASER FUSION STUDIES AT NRL		5. TYPE OF REPORT & PERIOD COVERED 6. PERFORMING ORG. REPORT NUMBER
7. AUTHOR(s) (10) J. McMahon, J. Orens, S. Bodner, D. Book, J. Boris, R. Decoste*, M. Emery, M. Fritts, J. Gardener, S. Gold, J. Grun, R. Lehmberg, E. McLean, P. Moffa**, D. Nagel, S. Obenschain, B. Ripin, J. Stamper, R. Whitlock, and F. Young		8. CONTRACT OR GRANT NUMBER(s)
9. PERFORMING ORGANIZATION NAME AND ADDRESS Naval Research Laboratory Washington, DC 20375		10. PROGRAM ELEMENT, PROJECT, TASK AREA & WORK UNIT NUMBERS 67-0859-A-0
11. CONTROLLING OFFICE NAME AND ADDRESS (11) 17 U. S. Department of Energy Washington, DC 20545		12. REPORT DATE October 8, 1980 13. NUMBER OF PAGES 21
14. MONITORING AGENCY NAME & ADDRESS(if different from Controlling Office) (12) 21		15. SECURITY CLASS. (of this report) UNCLASSIFIED 15a. DECLASSIFICATION/DOWNGRADING SCHEDULE

16. DISTRIBUTION STATEMENT (of this Report)

Approved for public release; distribution unlimited.

17. DISTRIBUTION STATEMENT (of the abstract entered in Block 20, if different from Report)

18. SUPPLEMENTARY NOTES

*Present address: IREQ Varennes Quebec, Canada
**Present address: TRW Redondo Beach, California
This research was supported by the U. S. Department of Energy.

19. KEY WORDS (Continue on reverse side if necessary and identify by block number)

Laser-fusion, Rayleigh-Taylor instability

20. ABSTRACT (Continue on reverse side if necessary and identify by block number)

The NRL group is studying the technical feasibility of high gain laser fusion pellets driven by low irradiance (10^{14} W/cm^2) multi-nanosecond lasers. In earlier experiments, it was shown that both absorption and hydrodynamic efficiencies were consistent with high gain pellet designs. In addition to extending this work to greater intensities and larger spot sizes, research is underway on the origins and magnitude of target preheating at low irradiance, on experimental and theoretical work on the issue of symmetry and into the related questions of Rayleigh-Taylor instability and mixing of layers in multi-layer targets. Substantial progress has been made in all of these areas: the rear surfaces of slab targets have been ablatively accelerated to velocities above 10^7 cm/sec with acceptably low levels of preheat and there is experimental evidence of smoothing of spatial non-uniformities in the laser profile on a transverse scale of 100μm or less.

DD FORM 1 JAN 73 1473 EDITION OF 1 NOV 65 IS OBSOLETE
S/N 0102-LF-014-6601

SECURITY CLASSIFICATION OF THIS PAGE (When Data Entered)

251 110

CONTENTS

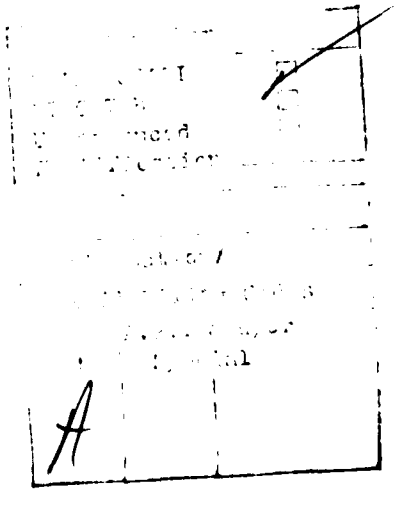

LASER FUSION STUDIES AT NRL
1—10 JULY 1980
BRUSSELS, BELGIUM
IAEA-CN-38/I-1

INTRODUCTION

In order for a laser fusion reactor to succeed in producing net energy gain high, gain pellets ($G \geq 100$) are necessary. This requirement for high gain imposes certain physics constraints. The pellet fuel must be efficiently imploded in a near-isentropic fashion to high final densities. From simple considerations the physics constraints on achieving high gain pellet performance are:

- overall coupling efficiency ($\eta_{absorption} \times \eta_{hydrodynamic}$) at least in the range of 7-10%
- very little preheat ($T_{fuel} < 4T_{Fermi}$)
- very good implosion symmetry ($\Delta V_f / V_f \sim 1$-2%)
- no significant de-symmetrization caused by Rayleigh-Taylor instability.

As was reported by our group two years ago at the Innsbruck meeting, our experiments at high laser intensities ($\geq 10^{15}$ W/cm^2) led us to conclude that pellet designs using shaped pulses rising to high intensities, at a one micron wavelength, did not look promising for high gain because of problems with preheat and coupling.[1] Accordingly, we decided to concentrate our efforts on investigating pellet concepts which employ longer duration laser pulses at lower peak intensities ($< 10^{14}$ W/cm^2).[2,3] In this paper, we will report on the progress we have made in studying the key issues of coupling efficiency, preheat, symmetry and stability for this laser fusion concept.

Rather than irradiate whole pellets for these physics studies, we use flat discs or foils (or multiple foils), irradiated from one side with typical laser spot sizes of 500μm to 1000μm. To produce a more uniform intensity profile, the targets are placed in the "near field" of the laser rather than at focus. Flat targets have some advantage over pellets, as a first generation of experiments:

- Less laser energy can be used than would be necessary to irradiate spheres.
- the back surface of the target is accessible for diagnostics. With a pellet, it is difficult to diagnose the interior much below the point where thermonuclear ignition occurrs:

Manuscript submitted August 15, 1980.

This flat geometry also has several obvious disadvantages when compared to a symmetrically imploded shell:

- edge effects may make it difficult to perform sufficiently one-dimensional experiments.

- there may be anomalous preheat effects which would not be present in a spherical target.

- small symmetry differences, which are important in implosions, may be difficult to measure in experiments which lack spherical convergence.

This paper will address the progress we have made in overcoming and/or evaluating these difficulties in the context of the pellet physics. A number of results from these experiments have already been reported; we will summarize these results but will concentrate mainly on recent progress.

OVERALL COUPLING EFFICIENCY

The laser to target coupling efficiencies have been measured with an array of calorimeters of various sorts; typically the laser absorption efficiency was 90% at 3×10^{12} W/cm^2 irradiance and declined to 55% at 7×10^{14} W/cm^2,[4] with a laser pulse length of 3-4 nsec. Particle energy and momentum were measured, for both the front surface plasma and the ablatively accelerated material at the rear surface, using minicalorimeters and charge collectors. With these detectors good overall energy accounting and momentum balance was obtained and hydrodynamic efficiencies as high as 20% were obtained.[5] Another method of detection was also attempted using ballistic pendula front and rear. Initially the pendulum results, while showing reasonable relative momentum balance, gave absolute momentum values considerably lower than the charge collector/minicalorimeter system. We have recently been successful in resolving this discrepancy with a series of double pendulum experiments, in which a second pendulum was used to measure the fraction of the incident particles which did not stick to the first pendulum, as well as mass ablated from the first pendulum. We believe that this is the first time that ballistic pendula have been accurately calibrated. The ballistic pendula results are now in quantitative agreement with the results measured with charge collectors and particle calorimeters. The high overall coupling efficiency at lower irradiance, (55-90%) x (20%) $\simeq$ (11-18%), is encouraging for the laser fusion concept.

We have also performed experiments to evaluate the question of edge effects, both by varying the spot size on slab targets while maintaining fixed irradiance and by using limited mass disc targets rather than slab targets. The conclusion of these experiments was that with small spots ($\lesssim$300μm) edge effects were significant but they became less important as the spot size was increased and at a spot size of 1000μm or larger they were not a significant factor. Spot size does require laser energies of a kilojoule in a 3ns pulse in order to reach irradiance levels in the mid-10^{13} W/cm^2 range.

PREHEAT QUESTIONS

To achieve high densities, the fuel must remain in a low isentrope during the spherical implosion. We have previously reported several results which confirm that we are, in fact, ablatively accelerating material,[4,5] on a cold isentrope. These results included; X-ray spectral measurements from 2 keV to 50 keV which showed a notable lack of high energy (10 keV) X-rays; particle detectors; and direct, time-resolved measurements of the rear surface brightness temperature.[6] Fast response (~1 ns) photomultipliers were used in conjunction with monochromators to give time resolved emission data in two spectral channels. The response of the two channels was also calibrated with a standard lamp, allowing a brightness temperature to be determined at the two wavelengths at any instant of time. Data such as shown in Figure 1 were obtained.

While temperatures remained low during the laser pulse, there was still a question as to whether there was any preheating of the rear surface due to particles from the heated front surface streaming around the target. We optically imaged the target onto the slit of a fast optical streak camera and measured the space and time resolved rear surface emission. Streaming did not occur for large foil targets or for discs whose dimensions were very large but for disc targets of about the same size as the laser spot, there was evidence of energy flowing around the disc.

There are three mechanisms for heating the rear surface of slab targets at low intensities: soft x-rays, shocks and thermal conduction. That shock heating has a role was verified by comparing the time history of the rear surface temperature of a single 4μm Al foil to another target with two Al foils, one 3.5μm thick and the second 0.5μm thick, separated by 200μm. The rear surface of the double target was significantly colder, indicating that shock heating was a significant effect for the single target of the same mass. These experiments appear capable of yielding important experimental data for pellet design on preheat effects. Comparison of the experimental results with calculations are in progress; the magnitude of the observed heating appears to be in reasonable agreement with preliminary calculations of what would be expected from these three mechanisms. Extrapolation to reactor-sized pellets indicate that fuel can be kept on a low isentrope ($E \lesssim 4\ E_F$), using low laser irradiance.

SYMMETRY QUESTION

Symmetry of the implosion appears to be a serious remaining issue for low irradiance pellet designs. A limit on velocity asymmetry of only a few percent implies an ablation pressure uniformity of the same order. There are several issues involved in understanding the impact of symmetry on the viability of laser fusion pellet designs:

- To what extent will the pressure profile in the ablation region reflect the laser intensity profile in the physically separated absorption region? Will there be smoothing of irregularities in the laser pattern, in terms of the resulting pressure profile, and over what transverse scale length?

- How uniform a laser pattern can be produced on the target surface and over what transverse scale lengths can the profile be controlled?

- Can diagnostics be developed for the disk experiments which will measure small, but significant, pressure and/or velocity gradients?

We have previously reported the results of simple experiments which qualitatively show smoothing of irregularities in the illumination pattern on a transverse scale of 100μm or less.[5]

A schematic of the layout of the Pharos II laser system is shown in Figure 2. This laser has produced over one kilojoule in a 3.5 ns pulse with an overall driver efficiency of 0.2%. The laser performance is largely due to the use of high gain (≥14%/cm) neodymium phosphate glass in the disc amplifiers.[7,8] There are a number of features of this laser design which were incorporated with the specific intent of producing uniform illumination on millimeter size targets:

- The energy density in the rod section of the laser is kept below 50% of the saturation flux. This allows spatial shaping of the oscillator pulse by the gain profile in the rods without time dependent changes in pulse shape.

- The beam is shaped by a hard or soft aperture after the final rod amplifier and this pattern is then sequentially relayed through the disc amplifiers and onto the focus lens. The propagation from the lens to target plane, including diffraction effects, was computed to generate a prescription for the spatial profile of the "soft" aperture.

- Care was taken in the design and its execution to minimize phase errors. At full power, the "B" integral is of order unity, so small scale self-focusing effects are wholly absent and whole beam self-focusing amounts to only a dynamic shift of $\lambda/6$ at the peak of the pulse. The residual phase errors were measured using wavefront shearing interferometry and found to consist primarily of one wave of spherical aberration. Tests with a prototype high power soft aperture showed a capability to compensate most of the spherical aberration as well as shaping of the amplitude profile.

The relationship between the laser intensity pattern and the foil targets' rear surface velocity pattern was measured by spatially resolving the Doppler shift of a short (~0.5 ns) second harmonic probe pulse reflected from the rear surface.[4] These early measurements showed smoothing of deliberately produced amplitude fluctuations but the technique was limited in two respects:

- it could only track the velocity profile early in time because of the absorption of the probe light as the rear surface warmed up.

- the $\Delta v/v$ resolution was relatively coarse, about 20%, because of the relatively small Doppler shifts and the probe bandwidth.

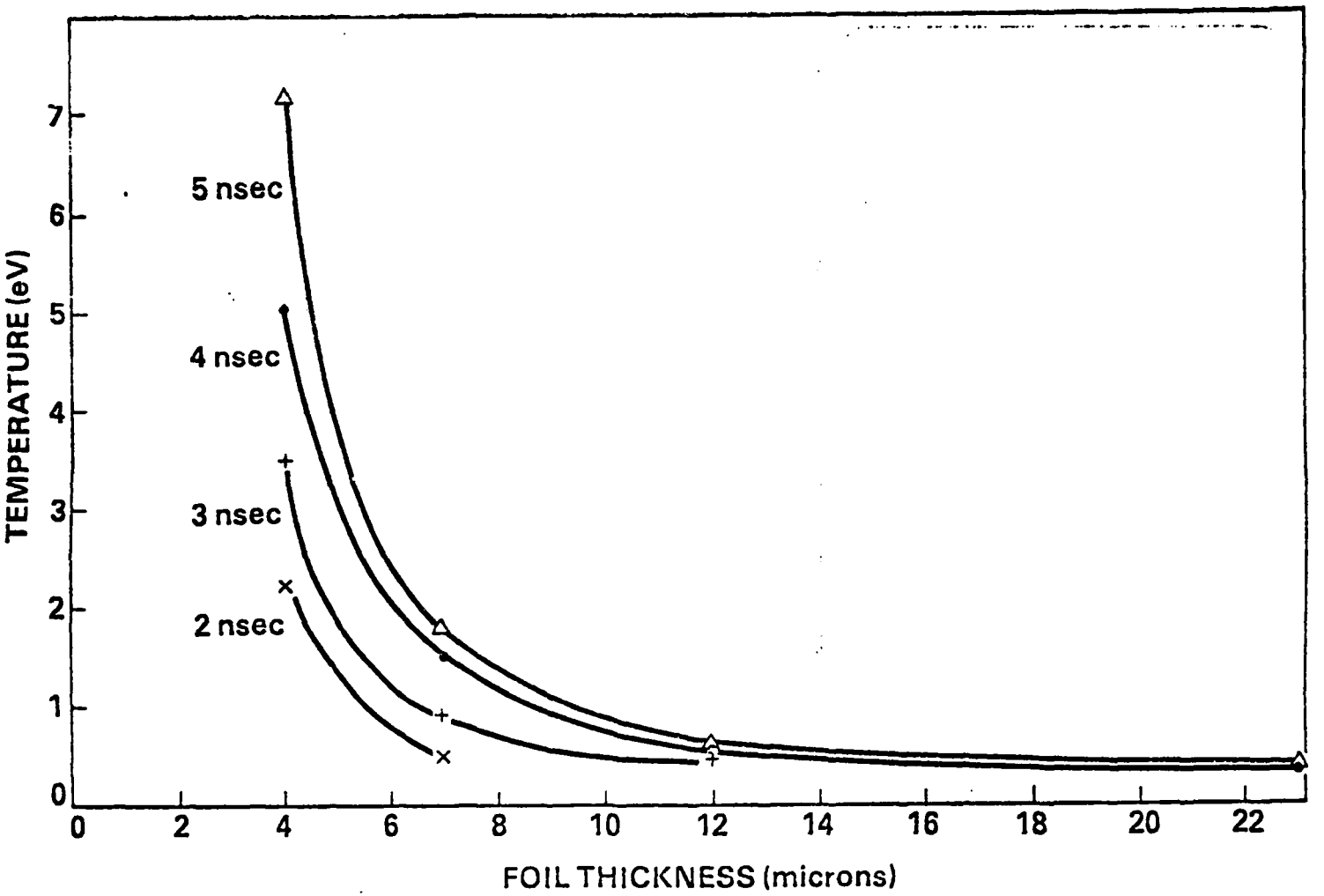

Fig. 1 — Measured rear surface temperature as a function of Aluminum target thickness at an irradiance of 5×10^{12} W/cm^2 in a 1mm diameter spot. The indicated times are times after the peak of the laser pulse. By 5 nsec after the peak acceleration of the rear surface has ceased.

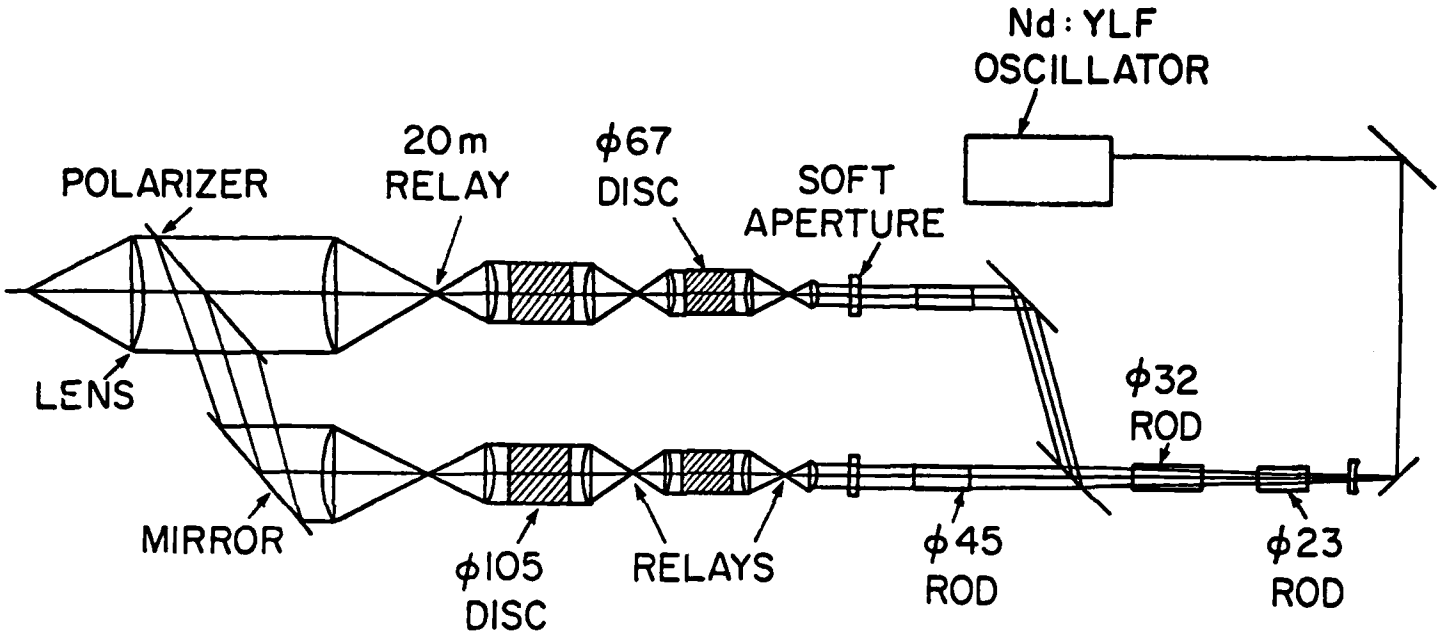

OPTICAL LAYOUT
(ISOLATION DELETED FOR CLARITY)

Fig. 2 — Optical layout of the Pharos II laser system. A Nd:YLF oscillator is used to match the phosphate glass amplifiers in wavelength. The orthogonally polarized 10.5 cm diameter beams out of the laser are expanded to 20 cm diameter by the final relay and combined using a dielectric polarizer. They are focused onto the target with an F/6 aspheric lens.

We have recently developed a diagnostic technique which circumvents both of these problems. A second foil is placed behind the first foil and the light emission is recorded from the second foil as it is impulsively accelerated by the first foil. In a separate experiment it was verified that this emission coincides in time with the time when the second foil begins to move. Sections of the first target which are ablatively accelerated to lower velocities will impact later and the streak record will provide a direct record of $v(r,t)$. By varying the separation of the two foils, the impact time can be chosen to be any time during or after the laser pulse. This diagnostic technique is in use to measure the sideways thermal conduction as a function of irradiance. As the irradiance is increased irregularities in the laser profile should be smoothed more effectively both by thermal conduction and an increase in the physical separation of absorption and ablation regions. The data shown in Figure 3 would seem to indicate that this is the case. The laser was operated at energies of 200J and 400J in 4ns which produced average irradiances of 6×10^{12} W/cm^2 and 1.2×10^{13} W/cm^2 for the two cases with the center of the beam masked by a strip of paper in both cases. This produced a pattern on target with a 7:1 intensity ratio. The streak record of the rear surface luminosity in the low irradiance case would indicate some smoothing but there was still a 2:1 velocity difference between the high intensity and low intensity regions. At the higher irradiance the smoothing is clearly better.

These results, while encouraging, are preliminary. They do indicate, however, that it appears possible to address the symmetry issue experimentally in flat target experiments.

OVERVIEW ON THEORETICAL INVESTIGATIONS OF STABILITY

In the theoretical area, substantial effort has gone into understanding the Rayleigh-Taylor instability and related but distinct asymmetry problems for spherical implosions. A fundamental concern for inertial confinement fusion is the severe energy penalties one must be willing to pay to design conservatively. There are four different circumstances where desymmetrizing instabilities can grow: in the ablation layer, at internal interfaces where materials of different density abut, at the buffer-shell interfaces which occur in multiple-shell pellets, and where the core shocks interact with density gradients and the pusher interface. To study ablation layer Rayleigh-Taylor modes we have used a fully nonlinear Eulerian computer model[1] and have developed special analytic and numerical tools to carry out meaningful resolved piggyback calculations of Rayleigh-Taylor growth for an analytically determined "quasi-static" equilibrium. To perform internal layer analyses we use a Lagrangian hydrodynamic model based on a two dimensional dynamically reconnectable grid of triangles. To study imploding shock stability we use a computational model based on the Chester-Chisnell-Whitham (CCW) approximation[2] and have discovered a class of closed-form theoretical self-similar one-dimensional models. Principal results include the discovery of Rayleigh-Taylor stable regimes for low-intensity laser-driven ablation; the simulations of the two layer pusher-fuel mix problem and the three-layer mix problem (a light fuel layer is separated from a denser pusher shell by a thin but very dense heat shield layer) and the definitive of a wide range of stability and symmetry issues related to shock collapse.

EFFECTS OF INCREASING LASER INTENSITY ON SYMMETRIZATION

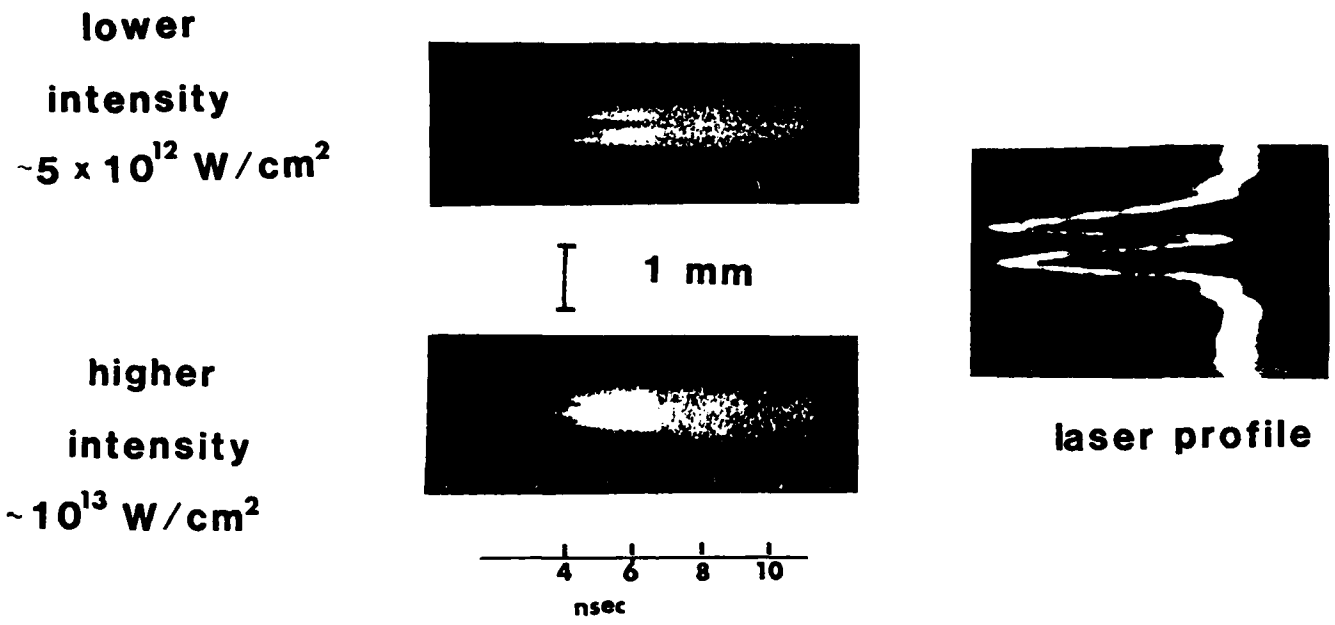

Fig. 3 — Streak camera photographs of the luminosity of the rear surface of a second foil placed 200μm behind the target foil. The laser intensity pattern was perturbed by masking the center of the lens with a strip of paper resulting in the laser patterns shown on the right of the figure. At lower intensity this results in the low target velocity in the center of the pattern. At higher intensity not only is the velocity higher (earlier time of arrival at the second foil) but the effect of the mask in the laser beam almost totally disappears.

INVESTIGATION OF THE STABILITY OF LASER-DRIVEN ABLATION LAYERS

Previous authors have investigated steady-state models for the ablation layer of laser-driven foils[10] and spherical implosions[11] and have considered the hydrodynamic stability of a laser-driven plasma.[12] Since the density and pressure gradients are opposite in sign in these ablation layers simple but incomplete analysis predicts that perturbations may grow exponentially there. Our earlier research into the "quasi-static" (time independent) ablation layer profiles has identified two distinct types of pressure profiles.[13] In the first case the pressure profile has the intuitively expected turning point and yields a very narrow region ($\sim .1\mu m$) where the density and pressure gradients are opposite in sign. In the second case the pressure profile does not turn over and continues to increase out to the critical surface. Here the region where the density and pressure gradients are opposite in sign is quite broad ($\sim 100\mu m$). Afanasyev et al.[2] have noted that the width of this region with opposed gradients can affect the growth rate of perturbations. In Reference 1 we pointed out the dilemmas encountered in attempting to properly treat the stability analysis for both theoretical and numerical calculations. In theoretical studies it is difficult to include the effects of convection, while in simulations the problem is sufficient resolution. In fact, simulations with rather poor resolution of the region with opposed gradients are seen to be Rayleigh-Taylor-unstable, but when the resolution is improved the growth rate becomes dramatically reduced. To date, limits of practicality have kept us from performing large scale, fully time dependent calculations with what we would consider to be the proper resolution. Previous piggyback calculations where a time-dependent perturbation is applied to a zeroth order equilibrium have attempted to solve this dilemma, but we are unaware of any with sufficient resolution from which to draw definite stability conclusions. A new piggyback formulation, the vorticity generation model has provided us with a mechanism for adding convection to our theoretical analyses and permits high enough resolution for an accurate assessment of stability for these and various other types of time-independent and time-dependent equilibria This formulation is especially convenient for both analytic and numerical analyses since it does not require calculation of the pressure perturbation. We have applied the VGM to various test problems and to "quasi-static" equilibria for CH foils irradiated at 10^{13} W/cm^2. We have discovered that equilibria with a narrow region of opposed gradients are Rayleigh-Taylor-stable while equilibria with a broad region are Rayleigh-Taylor-unstable. We have also used fully non-linear Eulerian and Lagrangian time-dependent models to calculate the slow evolution of these two types of "quasi-static" equilibria. At constant intensity "quasi-static" equilibria with a narrow region of opposed gradients tend to retain this character, while "quasi-static" equilibria with a broad unstable region evolve one-dimensionally into profiles with a much narrower potentially destabilizing region. Figure 4 shows the temporal evolution of these two types of equilibria. This encouraging result implies that configurations which are unstable to Rayleigh-Taylor modes in the ablation layer evolve toward stabler equilibria.

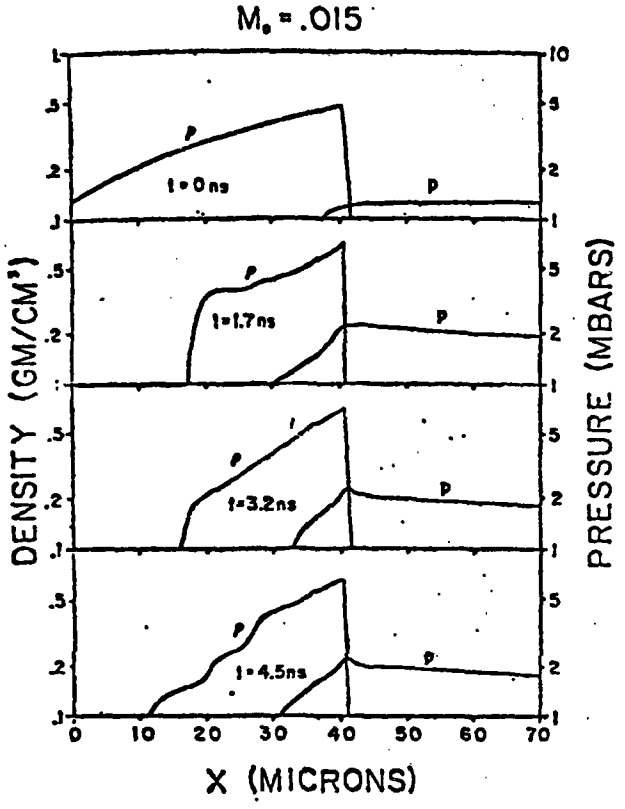

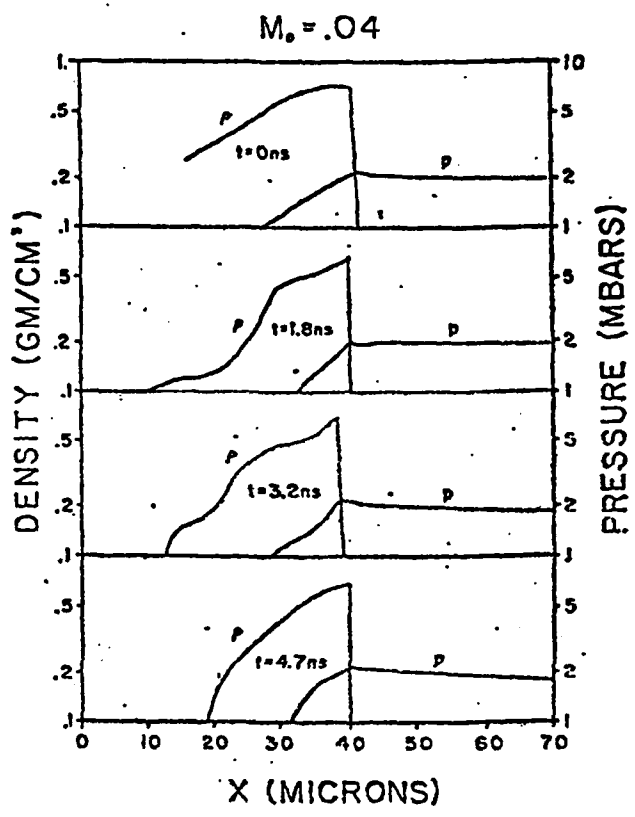

Case #1 $\frac{dP}{dx} > 0$ as x approaches x_c

$I = 10^{13}$ W/cm^2 (.8, .2) on 15μ CH foil

$S = 4 \times 10^{12}$ $g \approx 0.9 \times 10^{15}$ cm/sec^2

$\rho_{max} = .486$ gm/cm^3 $P_{max} = 1.20$ Mbar

$T\rho_{max} = 3.73$ ev $\Delta R \approx 53\mu$

$M_o = 0.015$ $N_o = 2606$

Case #2 $\frac{dP}{dx} < 0$ as x approaches x_c

$I = 10^{13}$ W/cm^2 (.8, .2) on 15μ CH foil

$S = 4 \times 10^{12}$ $g = 1.5 \times 10^{15}$ cm/sec^2

$\rho_{max} = .691$ gm/cm^3 $P_{max} = 2.16$ Mbar

$T\rho_{max} = 4.71$ ev $\Delta R \approx 40\mu$

$M_o = 0.04$ $N_o = 4560$

Fig. 4 — Temporal evolution of the two types of "quasi-static" equilibria with the same shell entropy.

INVESTIGATION OF THE INTERIOR LAYER RAYLEIGH-TAYLOR INSTABILITY

The interior layer Rayleigh-Taylor problem can occur at many different times and locations during the implosion of a complicated multiple shell target. The pre-ignition mix problem is the most familiar situation. As the fuel compresses up to its final density, the pusher decelerates to provide the compressional energy. Since the pusher density exceeds that of the fuel, the interface becomes unstable as soon as the acceleration due to convergence gives way to compressional deceleration. A three-layer mix problem also arises where a light fuel layer is separated from a denser pusher shell by a thin but very dense heat shield layer. In this three-layer problem short wavelength perturbations permit the upper and lower surfaces of the heat shield to move independently, so Rayleigh-Taylor instability can result even though overall stability is expected at long wavelength. In order to investigate the nonlinear regime of the Rayleigh-Taylor instability for these two- and three-layer mix problems we have developed a Lagrangian model which bases its fluid representation on a two-dimensional dynamically reconnectable grid of triangles.

Several flow features illustrated in Figure 5 are common to all simulations of the Rayleigh-Taylor instability performed with this model. First, the dense spike of fluid never attains a "free-fall" penetration rate because of the high efficiency of the vortex pair in transforming the downward vertical motion of the bottom of the spike into a lateral, spreading motion and, eventually, mixing in the vortices. Second, since the Helmholtz vortices dominate only after some amplitude a/λ is attained, the penetration rate in the nonlinear regime may depend on wavelength. Third, the secondary Helmholtz vortexes tend to further mix the already distorted interface, but the nonlinear flow is dominated by the original vortex pair. Fourth, both primary and secondary vortices appear to have little effect on mixing at the stable interface, and a bridge of dense fluid thins but remains stable. A heat shield would thin appreciably, but remain integral well into the nonlinear regime despite large mixing of the spike. Finally, the jetting which forms above the descending spike seems to be the primary means of mixing across the stable interface. This jet arises from the formation of a stagnation point at the junction of the flow into the spike from the upraised bridges to either side. The jet eventually collapses as the bridges then, form bubbles of trapped fuel.

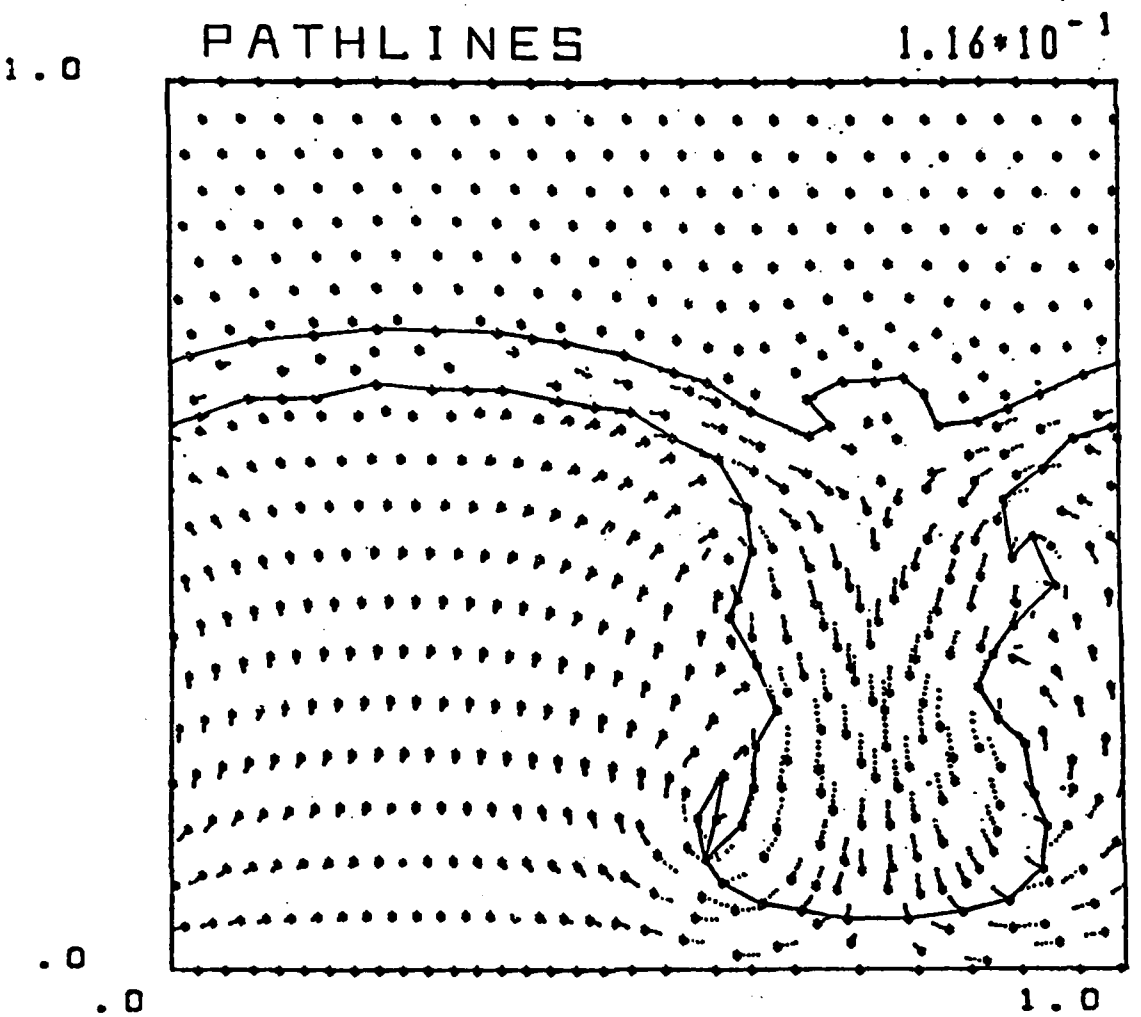

Fig. 5 — A frame from a movie of a Lagrangian simulation of the nonlinear phase of a three-layer-mix problem. A light fuel layer is separated from a denser ablator by an even more dense pusher shell. The flow is similar in many respects to the pusher-heat shield-fuel simulations.

SPHERICAL SHOCK IMPLOSION DYNAMICS AND STABILITY

The critical consideration for achieving a high degree of compression in a spherical implosion is to determine the symmetry requirements on the driver by finding the degree of symmetry that can be maintained during the implosion process. The motion of a converging shock wave can be computed with great accuracy by considering only the changes in the physical variables across the shock front and ignoring the motion behind the front. The shock front moves normal to the shock surface, so it may be treated as locally one-dimensional flow down a channel whose boundaries are determined by the trajectories of the shock front. These trajectories form imaginary ray tubes whose cross-sectional area may be related to the Mach number by the CCW approximation. Using this approximation

we have investigated a wide range of stability and symmetry issues related to shock collapse. For instance, we need to know how large the initial perturbations may be even for stable modes since the perturbation amplitude may not go to zero as fast as the average radius. The concept of stability in the sense of an exponentially growing or decaying perturbation does not apply to this particular problem. Also, for a given set of wavelengths, Mach number, and initial radius, can the collapse of the shock be timed so that the amplitude of any particular oscillating perturbation is near zero at the instant of collapse? The superposition of (individually) unstable modes may then be stabilized nonlinearly. Using our model, Figure 6 summarizes pictorally the temporal evolution of 8th order Legendre polynominal perturbations to a spherical shock, with amplitudes of 5% and 10% respectively. As the shock collapses toward the origin (from right to left with increasing time), the amplitude of the 10% perturbation seems to grow relative to the radius. After implosion by a factor of 5:1, the 10% perturbation become contorted whereas the 5% perburbation is still behaving within acceptable bounds. We have also investigated the stability of the special case of the Guderley solution for strong spherical shocks imploding into a medium having a power-law density profile. For each choice of the adiabatic index γ, there is a unique power-law target density profile for which the flow behind the shock is uniform (radial velocity proportional to radius). The linearized equations of motion separate completely in Lagrangian variables, yielding an exact solution which predicts instability for this class of implosion. The CCW approximation gives essentially the same result for the case of uniform density ahead of the shock (power-law with zero exponent), while for the case of a power-law with increasing density ahead of the shock it predicts a reduction in the growth rate (result valid for arbitrary γ).

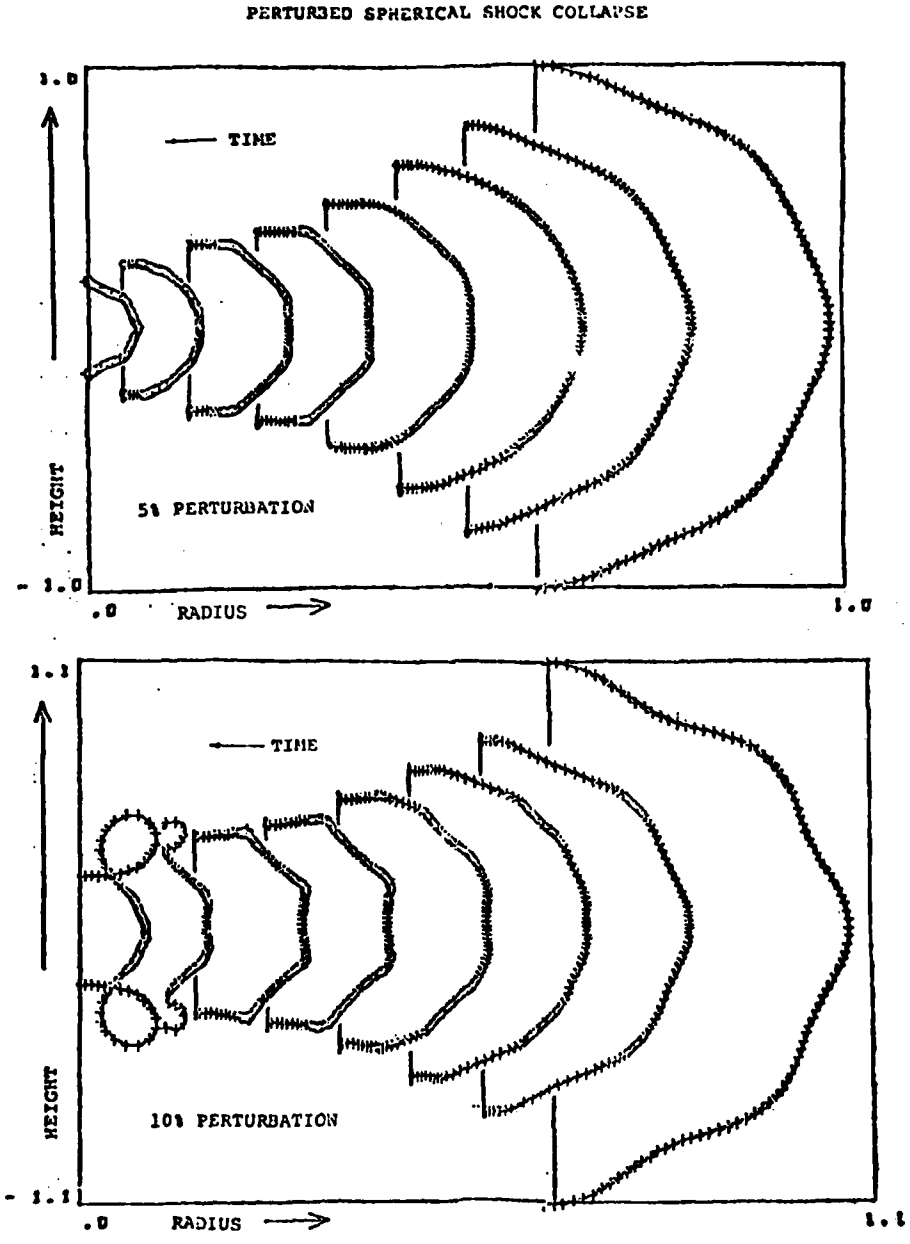

Fig. 6 — Solution using the C-C-W approximation for shock collapse of a spherical shock with an 8th order Legendre polynominal perturbation of 5% and 10% amplitude. The 5% perturbation becomes smaller at the same rate as the average radius remaining within acceptable bounds, while the 10% perturbation seems to grow relative to the average radius indicating an unstable behavior.

References

1. S.E. Bodner, et al. Paper IAEA-CN-37-B-3, 7th Int'l Conference on Plasma Physics and Controlled Fusion Research, Innsbruck, Austria, 23-30 Aug. 1978.

2. Yu. V. Afanasyev, et al. JETP Lett. 21, (1975), 150.

3. J. Nuckolls, Topical Meeting on ICF, Feb 7-9, 1978, San Diego, CA.

4. R. Decoste, et al., Phys. Rev. Lett. 42, 25 (18 June 1979), 1673.

5. B.H. Ripin, et al., Phys. Rev. Lett. 43, 5 (30 July 1979), 350.

6. E.A. McLean, et al., paper 4G2, 1980 IEEE Intl. Conf. on Plasma Science, May 19-21, 1980, Madison, WI.

7. J.M. McMahon, R.H. Lehmberg, Topical Meeting on ICF, Feb 7-9, 1978, San Diego, CA.

8. J.M. McMahon, R.H. Lehmberg, Topical Meeting on ICF, Feb 26-28, 1980, San Diego, CA.

9. K. Fang and B. Ahlborn, Phys. Fluids 22, (3), 416 (1979).

10. F.S. Felber, Phys. Rev. Lett. 39, 84 (1977).

11. S. Gitomer, R. Morse, and B. Newberger, Phys. Fluids 20, 234 (1977).

12. K. Brueckner, S. Jorna, and R. Janda, Phys. Fluids 17, 1554 (1974).
K. Brueckner, S. Jorna, and R. Janda, Phys. Fluids 22, 1841 (1979).

13. J.H. Orens, NRL Memo Report 4167 (1980).

DISTRIBUTION LIST

USDOE (50 copies)
P.O. Box 62
Oak Ridge, TN 37830

National Technical Information Service (24 copies)
U.S. Department of Commerce
5285 Port Royal Road
Springfield, VA 22161

NRL, Code 2628 (35 copies)

NRL, Code 4730 (100 copies)

NRL, Code 4700 (25 copies)

USDOE (6 copies)
Division of Laser Fusion
Washington, D.C. 20545
Attn: Dr. G. Canavan
Dr. R. Schriever
Dr. S. Kahalas
Dr. T. Godlove
Dr. D. Sewell
Dr. L. Killion

Lawrence Livermore Laboratory
P.O. Box 808
Livermore, CA 94551
Attn: Dr. D. Attwood, L481
Dr. W. Kruer, L545
Dr. J. Lindl, L32
Dr. C. Max, L545
Dr. A. Glass
Dr. L. Coleman
Dr. J. Nuckolls
Dr. W. Mead
Dr. N. Ceglio
Dr. R. Kidder

INTERNAL DISTRIBUTION

Code 4790 Dr. D. Colombant
Dr. W. Manheimer

Department of Physics and Astronomy
University of Maryland
College Park, MD 20740
Attn: Dr. H. Griem

Los Alamos Scientific Laboratory
Los Alamos, NM 87545
Attn: Dr. R. Godwin
Dr. S. Gitomer
Dr. J. Kindel

University of Rochester
Rochester, NY 14627
Laboratory for Laser Energetics
Attn: Dr. J. Soures
Dr. W. Seka

KMS Fusion
3941 Research Park Drive
P.O. Box 1567
Ann Arbor, MI 48106
Attn: Dr. F. Mayer

Institut fur Plasmaphysik
8046 Garching
Bei Munchen
West Germany
Attn: Dr. R. Sigel

National Research Council
Division of Physics
100 Susser Drive
Ottawa K1A-0R6, Canada
Attn: Dr. J. Alcock

University of Quebec
INRS Energie
Case Postale 1020
Varennes, Quebec
Attn: Dr. T. Johnston
Dr. R. Decoste

Rutherford Laboratory
Chilton, Didcot
Oxon OX110QX
England
Attn: Dr. M. Key
Dr. T. Raven

Sandia Laboratory
Albuquerque, NM
Attn: Dr. K. Matzen
Dr. J. Anthes
Dr. R. Palmer

Institute for Laser Engineering
Osaka University
Suita Osaka, 565
Japan
Attn: Dr. C. Yamanaka

Shanghai Institute of Optics and Fine Mechanics
Academia Sinica
Shanghai, PRC
Attn: Prof. Gan Fu-xi
Prof. Yu Wen-yan
Prof. Xu Zhi-zhan
Prof. Deng Xi-ming
Prof. Tan Wei-han
Mr. Pan Cheng-min

Soreq Nuclear Center
Yavne, Israel
Attn: Dr. A. Krumbein

INTERNAL DISTRIBUTION

Code 4040 J. Boris
J. Gardener
J. Orens

Dr. James Lunney
Dept. of Pure and Applied Physics
Queens University
Belfast, N. Ireland

Defense Technical Information Center (12 copies)
Cameron Station
5010 Duke Street
Alexandria, VA 22314

Dr. J. Weale (2 copies)
AWRE Aldermaston
Berkshire, England 55811